Deep–Sea Research II 218 (2024) 105428

Contents lists available at ScienceDirect

Deep-Sea Research Part II

journal homepage: www.elsevier.com/locate/dsr2

Exploring sea ice transport dynamics at the eastern gate of the Ross Sea

Naomi Krauzig [a,b], Daniela Flocco [c,*], Stefan Kern [d], Enrico Zambianchi [e,b]

[a] Dipartimento di Scienze della Vita e dell'Ambiente, Università Politecnica delle Marche, Ancona, Italy
[b] Consorzio Nazionale Interuniversitario per le Scienze del Mare, Roma, Italy
[c] Dipartimento di Scienze della Terra, dell'Ambiente e delle Risorse, Università degli Studi di Napoli "Federico II", Napoli, Italy
[d] University of Hamburg, Hamburg, Germany
[e] Dipartimento di Scienze e Tecnologie, Università degli Studi di Napoli "Parthenope", Napoli, Italy

ARTICLE INFO

Handling Editor: Dr W Smith

Keywords:
Ross Sea sea ice transport
Antarctic sea ice dynamics
Zonal flux
Teleconnections
Wind-driven forcing

ABSTRACT

As Antarctic sea ice extent continues to reach record lows, significant efforts have been directed towards understanding the underlying processes and their regional differences within the Southern Ocean. Here, we explore the dynamics of zonal sea ice transport at the eastern gate of the Ross Sea from 1988 to 2023 using GIOMAS-model and ERA5-reanalysis data. Our analysis reveals a modest overall increase in eastward sea ice transport (3.721 ± 0.672 km^3/month per decade), with diverging trends in the coastal and open ocean zones. Driven by easterly winds and the Antarctic Slope Current, the predominant westward transport in the coastal region experienced a significant rise during the early 2000s, followed by a steep decline post-2011. Conversely, driven by the Antarctic Circumpolar Current, the strong open-ocean transport exhibited a moderate increase towards the Amundsen Sea until the late 1990s, which was interrupted by a reversal in 2007. The variability of zonal sea ice transport and its underlying conditions (sea ice concentration, thickness, and zonal drift) revealed considerable shifts throughout the different decades and on seasonal scales. During austral winter, approximately half of the zonal sea ice transport variability seems to be driven by large-scale teleconnections, including the Southern Annular Mode, Southern Oscillation Index, Amundsen Sea Low and the Zonal Wave 3 with considerable impacts on the wind stress field. Whereas during summer, the Southern Oscillation Index emerges as the dominant driver, exhibiting a significant positive correlation ($r=0.55$, $p<0.001$) that reflects the influence of the El Niño-Southern Oscillation, while other teleconnections play minimal roles. Our study highlights the complex nature of sea ice transport through the eastern gate of the Ross Sea towards the Amundsen Seas, where contrasting climatic conditions are known to occur.

1. Introduction

Antarctic sea ice is a key component of the global climate system (IPCC SROCC, 2020), regulating heat, momentum and gas exchanges between the atmosphere and the ocean (Wang et al., 2023). As such, it influences marine ecosystems (Massom and Stammerjohn, 2010), weather patterns, the global carbon cycle (Rysgaard et al., 2011), dense water formation and thermohaline circulation, and prevents ice shelf disintegration (Massom et al., 2018; Van Achter et al., 2022).

Since the onset of the satellite era in 1978, Antarctic sea ice has been extensively monitored, revealing complex variability patterns (Parkinson and Cavalieri, 2012; Nihashi and Ohshima, 2015; Fogt et al., 2022). Satellite data show that the extent of sea ice gradually increased from 1979, reaching a record maximum between 2012 and 2014, followed by a sharp decline to historically low levels in 2016 (Meehl et al., 2019; Eayrs et al., 2021; Parkinson and DiGirolamo, 2021), a trend that has persisted to the present (Purich and Doddridge, 2023; Jena et al., 2024). While several model-based studies suggest a slight increase in sea ice thickness and volume, no definitive trend has been established (Massonnet et al., 2013; Holland et al., 2014).

This change in Antarctic sea ice extent trends has been attributed to intricate interactions between physical drivers, including atmospheric conditions (Schlosser et al., 2018; Wang et al., 2019), ocean temperatures (Stuecker et al., 2017; Eayrs et al., 2019; Purich and Doddridge, 2023; Jena et al., 2024), and large-scale teleconnections (Raphael et al., 2016; Wang et al., 2019) such as the Southern Annular Mode (SAM), El

* Corresponding author.
E-mail addresses: n.krauzig@staff.univpm.it (N. Krauzig), daniela.flocco@unina.it (D. Flocco), stefan.kern@uni-hamburg.de (S. Kern), enrico.zambianchi@uniparthenope.it (E. Zambianchi).

https://doi.org/10.1016/j.dsr2.2024.105428
Received 31 May 2024; Received in revised form 10 October 2024; Accepted 11 October 2024
Available online 11 October 2024
0967-0645/© 2024 The Authors. Published by Elsevier Ltd. This is an open access article under the CC BY-NC-ND license (http://creativecommons.org/licenses/by-nc-nd/4.0/).

Niño–Southern Oscillation (ENSO) and the Amundsen Sea Low (ASL). However, currently no consensus exists on the primary mechanisms driving this change (Eayrs et al., 2019), and relevant works have pointed out that no single driver can explain the observed variability (Stroeve et al., 2016).

Furthermore, overall sea ice extent (SIE) trends in the Southern Ocean concealed significant regional differences (Turner et al., 2022), indicating that it is crucial to examine the different seas within the Antarctic region separately. The overall SIE increase observed until 2014 was mainly a result of a reduction in the Amundsen-Bellingshausen Seas counterbalanced by a prevailing expansion in the Ross Sea (Turner et al., 2015; Parkinson and DiGirolamo,2021; Jena et al., 2024). During this period, the Ross Sea was considered to have one of the most stable variability patterns around Antarctica, increasing in extent over recent decades. Whereas after 2015, the anomalous low expansions were especially prominent in the Ross Sea (Turner et al., 2022). This pattern of variability continued, culminating in the Antarctic sea ice extent reaching its observed minimum in February 2023 (Jena et al., 2024). The anomalies leading to this minimum were linked to oceanographic preconditioning factors (positive temperature anomalies) and, in the Ross Sea, by the persistence of polar cyclones and the early onset of El Niño (Jena et al., 2024).

Here, we focus on the evolution in the past 36 years of these regional dynamics and investigate the related sea ice transport in the Ross Sea. As pointed out by Abernathey et al. (2016), from an oceanographic perspective, sea ice transport, rather than extent, matters most. Harboring the Ross Ice Shelf Polynya, the largest recurring polynya in Antarctica (Kern, 2009; Nihashi and Ohshima, 2015), considerable amounts of sea ice are produced in and advected from the Ross Sea each season (Martin et al., 2007; Tamura et al., 2016; Nihashi et al., 2017, 2024). While the subsequent brine rejection is locally driving formation of dense shelf waters (Williams et al., 2008), the precursor of Antarctic Bottom Water (AABW, see Rintoul, 2007; Ohshima et al., 2013), the advected sea ice modifies water masses reaching the northern ice edge. In this region, the prevailing southerly winds lead to considerable meridional sea ice transport, which influences the volume and properties of Antarctic Intermediate Water (AAIW) and Subantarctic Mode Water (SAMW) at the northern edge where the sea ice melts (Abernathey et al., 2016; Haumann et al., 2016). Additional studies concentrate also on the north-south sea ice flow to explain the observed seasonal long-term patterns in the Ross Sea-Amundsen Sea, which are linked to the structure of the Southern Annular Mode (Schroeter et al., 2023).

Considering the significance of the aforementioned water masses, increasing attention has been directed toward changes in meridional sea ice export, whereas the zonal transport within the Ross Sea has been comparatively understudied. This work aims to provide insight into this transport, focusing on the sea ice flux through the eastern gate of the Ross Sea, defined here as the 150°W meridian. This insight is significant, considering the dynamic interplay between the Ross and Amundsen Seas, where contrasting climatic conditions are known to occur (Smith et al., 2012; Coggins and McDonald, 2015; Fogt et al., 2022).

By using simulation results from the Global Ice-Ocean Modeling and Assimilation System (GIOMAS) model (Zhang and Rothrock, 2003), we here investigate the variability of this sea ice transport in the area of the eastern gate, aiming to provide insight into the occurring dynamics in the Ross Sea and its significance in a larger framework. Section 2 describes the data and the methodology used to analyze the required sea ice properties. The variability of the properties and the relevant volume flux are presented in Section 3 alongside a preliminary comparison with potential drivers. Finally, the outcome and significance of these findings are discussed in Section 4.

2. Data and methods

A set of modeled GIOMAS data was utilized to analyze sea ice dynamics in the Ross Sea and to calculate the corresponding sea ice flux through the determined eastern gate. The potential influence of climatic and local drivers was examined utilizing relevant large-scale teleconnection indices and atmospheric data derived from the ERA5 reanalysis dataset.

2.1. Sea ice data from GIOMAS

In this study we used monthly sea ice motion, concentration and thickness data with a spatial resolution of 0.8°x0.8° from the GIOMAS model by the Polar Science Center of the University of Washington (http://psc.apl.washington.edu/zhang/Global_seaice/data.html), covering the years 1988-2023.

GIOMAS is based on the Parallel Ocean Model (POM) coupled with a 12-category Thickness and Enthalpy Distribution (TED) sea ice model (Zhang and Rothrock, 2003), which simulates sea ice ridging processes. It is driven by NCEP/NCAR reanalysis data and assimilates sea ice concentration, as detailed in Lindsay and Zhang (2006). The model's sea ice thickness has been shown to align well with satellite observations in the Arctic (Shi et al., 2021). Although GIOMAS does not perfectly reproduce absolute sea ice thickness from satellite altimeter observations on a pan-Antarctic scale, it captures the observed variability and long-term trends in our region of interest effectively (Liao et al., 2022).

While sea ice thickness can be derived from satellite laser altimeters (ICESat, ICESat-2) and radar altimeters (Envisat, CryoSat-2, among others), existing products do not cover the time period relevant to our study. Furthermore, uncertainties in these retrievals are significant and often challenging to quantify due to limited knowledge of Antarctic snow cover (Kern et al., 2015).

Since GIOMAS assimilates satellite data (Lindsay and Zhang, 2006), we deliberately excluded the data from 1979 to 1987 to avoid the high uncertainty arising from the transition between the SMMR satellite (1978-1987) and the SSM/I satellite, as discussed by Haumann et al. (2016). For the remainder of the period, the GIOMAS data show strong agreement with satellite-derived sea ice concentration from the National Snow and Ice Data Center (see Fig. S1 in the supplementary material).

2.2. Zonal sea ice transport calculation

In order to examine the flux across the eastern gate of the Ross Sea, we calculated the sea ice transport through the longitudinal section of 150°W between the latitudes 60°S and 76°S. This longitudinal section is based on the geographical eastern border of the Ross Sea, while the latitudinal range is based on the maximum climatological seasonal sea ice extent (see Fig. S2).

The sea ice volume flux (Fv) across this section was calculated from the integral of the zonal velocity component of the ice (u), sea ice thickness (h) and the sea ice area (A), which is derived from the sea ice concentration (c) and the area of each grid cell (a) according to the following equation:

$$F_v(i) = \sum_{i=1}^{N} u_i(a\, c_i)h_i$$

where i corresponds to the monthly time series from January 1988 to December 2023 and N to the number of grid cells along the gate. The flux gate along the selected 150°W section spans a length of 1776 km. Positive fluxes refer to the export of sea ice from the eastern gate of the Ross Sea towards the Amundsen Sea, while negative fluxes refer to the westward import of sea ice.

2.3. Wind data from ERA5

To assess local wind-driven forcing and calculate the Zonal Wave 3 teleconnection index (see 2.4), monthly atmospheric data from the ERA5 reanalysis dataset (Hersbach et al., 2023a, 2023b) by the European Centre for Medium-Range Weather Forecasts were used. Covering

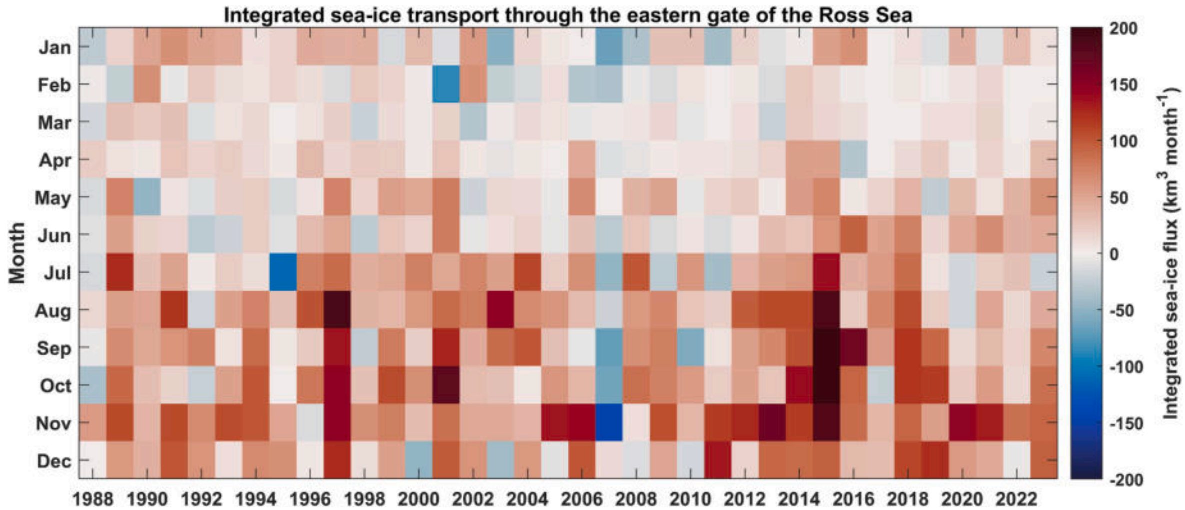

Fig. 1. Intra-annual time series of the integrated zonal sea ice volume flux across the eastern gate. Positive (red color) fluxes refer to the export of sea ice from the eastern gate of the Ross Sea towards the Amundsen Sea, while negative (blue color) fluxes refer to the westward import of sea ice.

the same time span of 1988–2023, the zonal (u10) and meridional (v10) surface wind components at 10m height and the meridional wind component (v) at 500 hPa level were selected.

2.4. Assessment of local wind-driven forcing

The surface wind components and the corresponding wind magnitude ($U = \sqrt{u10^2 + v10^2}$), were used to calculate the surface wind stress (τ) and Ekman transport (M_E) as follows:

$$\tau = \rho_{air} C_d U^2 \quad \text{and} \quad M_E = \frac{\tau}{\rho_{sea} f}$$

where $\rho_{air} = 1.35$ kg/m^3 is the air density, C_d the drag coefficient (Lüpkes and Birnbaum, 2005) accounting for sea ice cover and where $\rho_{sea} = 1027$ kg/m^3 is the water density and $f = 2\Omega \sin(\theta)$ is the Coriolis parameter with θ = latitude and $\Omega = 7.27 \times 10^{-5}$ s^{-1} is the earth's angular velocity.

While both zonal (east-west) and meridional (north-south) components of wind stress and Ekman transport were calculated, the corresponding statistical analysis (see 2.6.) focused mainly on the zonal components to assess the wind-driven impact on the eastward sea ice transport.

2.5. Assessment of potential large-scale drivers

The potential influence of large-scale teleconnections on the zonal sea ice transport was examined through correlational analysis of the normalized time series, spatio-temporal zero-phase and best-lag correlation and covariance analysis. The following monthly and seasonal indices were used:

a) The **Southern Annular Mode (SAM)**, the principal mode of atmospheric variability in the Southern Hemisphere, which is quantified by the zonal pressure difference between 40°S and 65°S (Marshall, 2003). The Marshall SAM index, reflects the north-south movement of westerly winds around Antarctica, and is derived from station-based measurements and provided by the British Antarctic Survey (BAS; http://www.nerc-bas.ac.uk/icd/gjma/sam.html).
b) The **Southern Oscillation Index (SOI)**, which measures large-scale pressure patterns in the tropical Pacific, encapsulating El Niño and La Niña phenomena. After confirming the consistency with the Niño 3.4 index (available at https://psl.noaa.gov/data/timeseries/month/Nino34), here we used the standardized SOI index, based on the observed sea level pressure (SLP) differences between Tahiti and Darwin, is available from the National Center for Atmospheric Research (NCAR; https://climatedata guide.ucar.edu/climate-data/southern-oscillation -indices-signal-noise-and-tahitidarwin-slp-soi).
c) The **Amundsen Sea Low (ASL)**, which characterizes the low-pressure system near the Amundsen and Bellingshausen Seas and its impact on local climate and sea ice conditions (Raphael et al., 2016). A deeper or more intense ASL is often associated with warmer air and sea temperatures in the West Antarctic region and can disrupt typical sea ice formation and dynamics (Hosking et al., 2013; Coggins and McDonald, 2015; Guo et al., 2020). Here we utilized the regional pressure anomaly provided by BAS (https://scotthosking.com/aslindex), which is calculated by subtracting the ASL actual central pressure from the area-averaged pressure over the ASL domain (170°-298° E, 80°-60° S).
d) The **Zonal Wave 3 Pattern (ZW3)**, which characterizes a prominent atmospheric wave pattern in the Southern Hemisphere mid-latitudes, featuring three alternating high and low-pressure systems encircling the continent (Raphael, 2004; Goyal et al., 2021). According to the latter, ZW3 influences regional climate and sea ice conditions by modulating atmospheric circulation, affecting wind patterns and temperature distributions over the Southern Ocean. Here, we utilized the ZW3 index derived from Empirical Orthogonal Functions (EOF, see 2.6) of the 500 hPa meridional wind anomalies, calculated between 40°S and 70°S, following the methodology of Goyal et al. (2022). Derived from ERA5 (Hersbach et al., 2023a), the first two principal components from the EOF analysis were employed to compute the ZW3 magnitude and phase.

2.6. Statistical analysis

The spatio-temporal variability of the mentioned data was studied by analyzing the monthly and interannual geographical and climatological distributions of averages, anomalies and trends of the entire Southern Ocean and across the selected eastern gate (150° W) of the Ross Sea. If not indicated otherwise, all time series (monthly, seasonal, yearly) were based on the spatial average of this area over the entire study period.

In agreement with the climatological fields of sea ice conditions (see Fig. S4), summer and winter seasons were based on the periods December to February and June to August, respectively. Anomalies were calculated by subtracting the monthly climatological mean for each month, effectively removing the seasonal cycle. Lastly, to compare the distribution over time, 3 quasi-decades (1988-1999; 2000-2011; 2012-

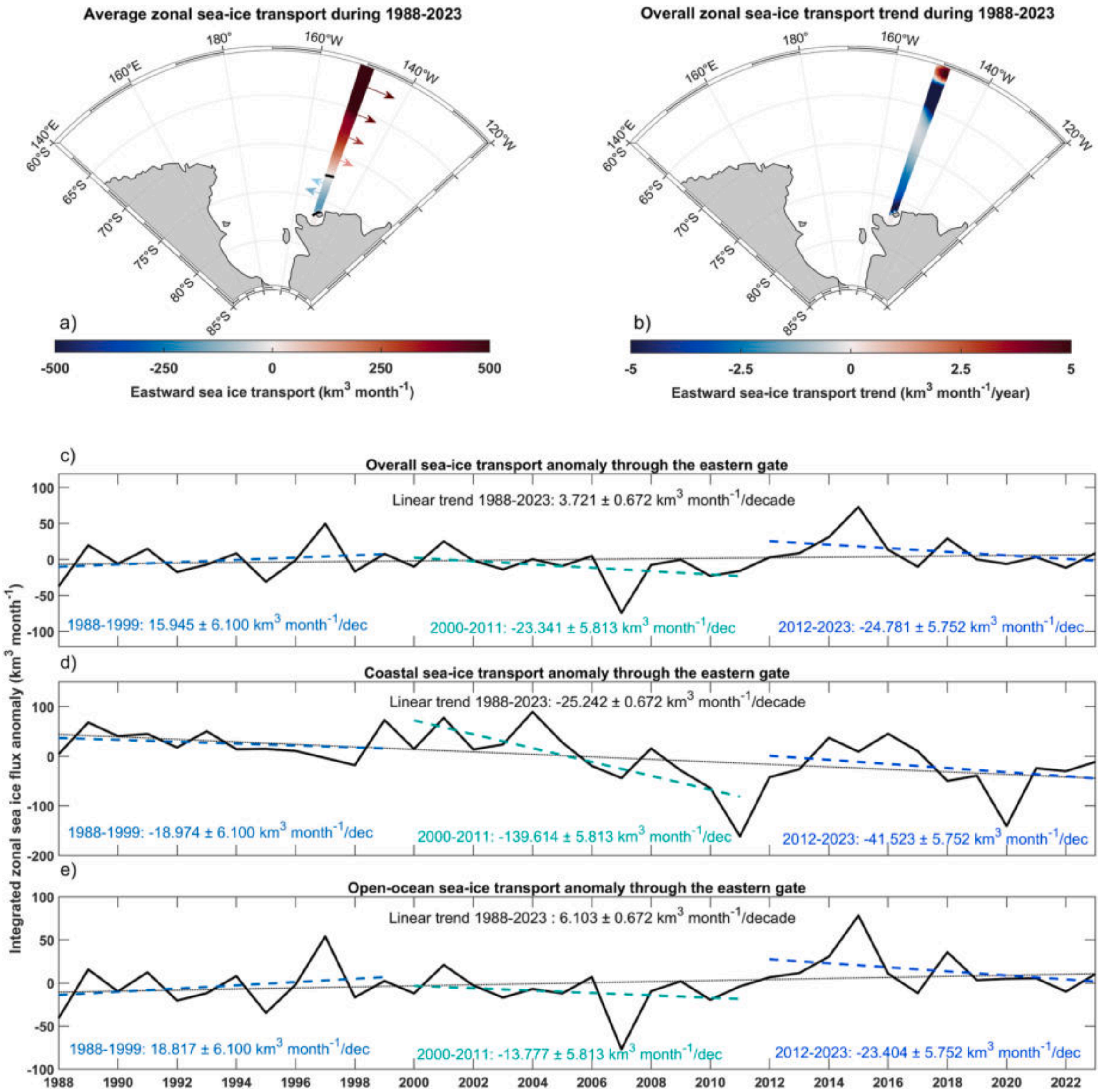

Fig. 2. Spatial distribution of the (a) average zonal sea ice transport across the buffered (±1 deg. longitude) eastern gate with sketched arrows indicating the direction and (b) its overall linear trend during 1988–2023. Positive (red color) fluxes denote export of sea ice through the eastern gate of the Ross Sea towards the Amundsen Sea, while negative (blue color) fluxes denote import of sea ice into the Ross Sea from the Amundsen Sea. The corresponding integrated time series of the (c) overall, (d) coastal (south of 72°S) and (e) open-ocean (north of 72°S) sea ice transport anomaly through the eastern gate is shown together with the linear trends for the entire period (black) and the ~decadal periods (color).

2023) as displayed in Figs. 2–5 were defined. Within each 12-year interval, the individual seasons were also examined.

The dominant spatio-temporal features of the zonal sea ice transport and the 500 hPa wind anomalies were examined using Empirical Orthogonal Function (EOF) analysis (Bjoernsson and Venegas, 1997), based on the respective detrended dataset. This method allows for the identification of key modes of variability by decomposing the dataset into principal components, thus highlighting the most significant and physically interpretable patterns that explain the majority of the variance. The first 3 EOF modes and Principal Components (PC) were examined to interpret the bulk of the variability, facilitating the identification of coherent patterns in sea ice transport that may be linked to potential large-scale drivers.

Trend estimation and de-trending was based on ordinary least squares linear regression with statistical significance set at the 95% confidence level. The corresponding uncertainties were defined by standard errors, whereas the statistical significance of the trends was examined through the Mann-Kendall test (Mann, 1945; Kendall, 1962). This test serves to identify the presence of a monotonic trend within a chronological series for a specific variable. The test's nonparametric nature, resistance to outliers, and focus on monotonic trends make it suitable for datasets where the normal distribution cannot be assumed, or where extreme values may skew the results of parametric tests.

The relationship between different variables was quantified using the Pearson correlation coefficient (r), with statistical significance determined by the p-value. Throughout this work, correlations with $p \leq 0.05$ were considered statistically significant. To further quantify the relationship, the Root Mean Square Error (RMSE) and Mean Absolute Error (MAE) were used to assess the magnitude of differences between them. Further details on the statistical analysis and relevant equations can be found in the supplementary material.

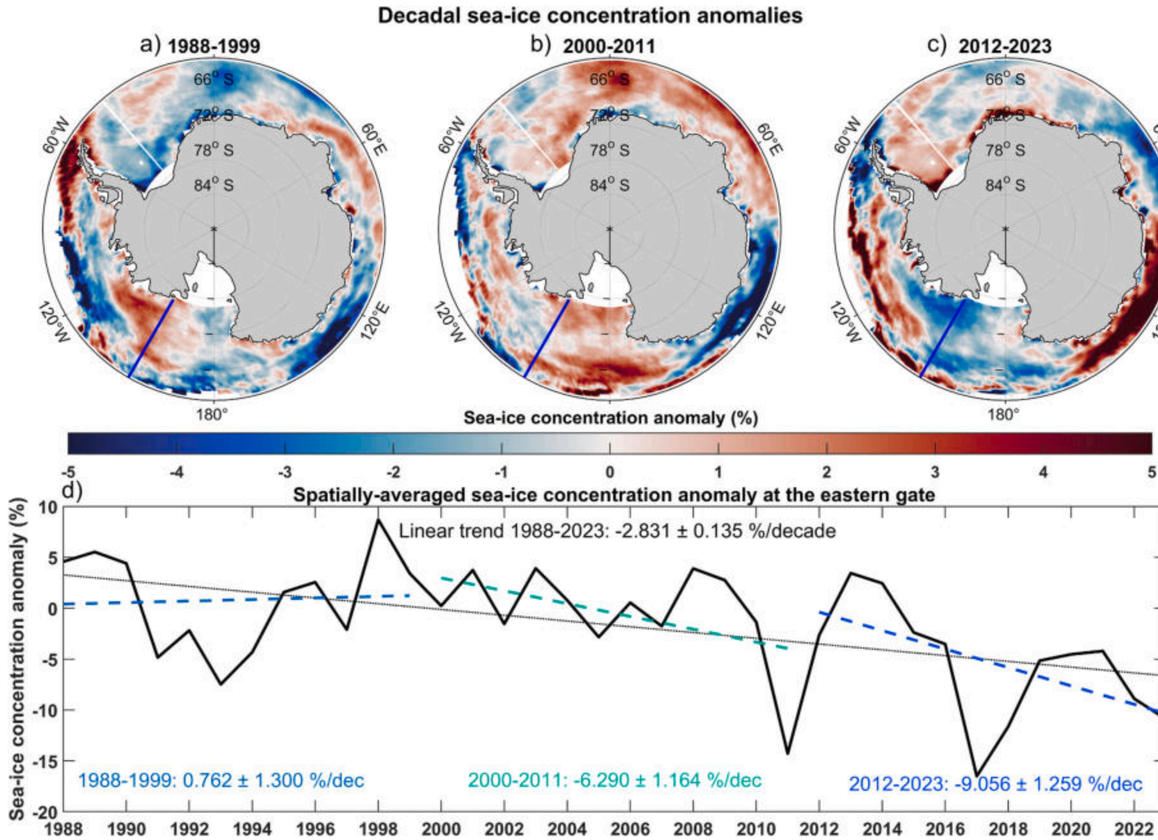

Fig. 3. Spatial distribution of the de-seasoned sea ice concentration anomalies during (a) 1988–1999, (b) 2000–2011 and (c) 2012–2023. The seasonal climatological fields of the sea ice concentration can be seen in Fig. S2a in the supplementary material; (d) Yearly values of the spatially-averaged anomalies through the selected eastern gate with trends per individual ~ decadal period (colored dashed lines) and trend for the entire time span (black dotted line). The longitudinal section of the eastern gate is indicated with a thick blue line in the spatial maps (a)–(c).

3. Results

Here we examine the intricate dynamics of sea ice transport at the eastern gate of the Ross Sea (along the 150°W meridian), differentiating between long-term trends, decadal variations, and seasonal fluctuations. Additionally, we distinguish between coastal and open ocean regions, each of which is governed by distinct atmospheric and oceanic drivers.

3.1. *Insight into the zonal sea ice transport through the eastern gate of the Ross Sea*

Our analysis indicates that the zonal sea ice transport through the eastern gate of the Ross Sea has maintained a predominantly eastward trajectory over the past four decades. However, this transport is subject to marked seasonal and interannual variability. The integrated sea ice volume flux (Fig. 1) tends to be stronger during the austral winter, with substantial fluctuations occurring throughout the time series. Specific periods stand out with particularly strong sea ice transport. August 1997 and July–November 2015 exhibit pronounced eastward transport, with fluxes exceeding 200 km^3 $month^{-1}$. Conversely, July 1995, February 2001 and November 2007 display significant westward transport, with values reaching -150 km^3 $month^{-1}$.

The integrated sea ice volume flux across the entire gate, however, concealed contrasting spatial conditions. As shown in Fig. 2a, the general zonal sea ice transport exhibits distinct patterns between the coastal area and the open ocean.

Near the coast, until approximately 72° S, a moderately westward transport of sea ice from the Amundsen Sea towards the Ross Sea is observed. This westward movement is likely influenced by prevailing easterly winds and the Antarctic Slope Current.

Conversely, north of 72° S, away from the coastal influence, a pronounced eastward transport of sea ice towards the Amundsen Sea is evident. This pattern aligns with expected dynamics under the influence of the Antarctic Circumpolar Current (ACC) and dominant westerly winds, demonstrating the significant role of the general large-scale circulation pattern in shaping sea ice distribution in the region.

The clear distinction between the coastal area and the open ocean aligns well with the sea ice conditions described by Assmann et al. (2005), who noted a transition from westward to eastward drift around the same latitude, reaching the eastern Ross Sea (165°W) during 1978–2001.

These contrasting dynamics result also in diverging zonal transport trends over the past four decades. While the overall integrated sea ice volume flux shows a modest increase in eastward transport of 3.721 (±0.672) km^3 $month^{-1}$ per decade (Fig. 2c), this general trend masks opposing behaviors in the coastal and open-ocean regions.

Over the entire period from 1988 to 2023, the integrated open-ocean and coastal sea ice flux anomalies showed trends of ~6 and ~-25 km^3 $month^{-1}$ per decade, respectively. However, instead of a general long-term intensification of sea ice export in the open ocean and sea ice import in the coastal area, we observe notable shifts (Fig. 2c-e).

In particular, the coastal import of sea ice from the Amundsen Sea to the Ross Sea increased significantly during the early 2000s, reaching anomalies over -160 km^3/month in 2011. This was followed by a steep decline, and by 2016, the coastal transport values were approximately 45 km^3/month lower than the long-term average (see Table S1). The weakened coastal sea ice import from the Amundsen to the Ross Sea aligns with findings from Silvano et al. (2020), who reported a significant decline in sea ice import between 2015 and 2018, driven by a combination of unusual climate drivers.

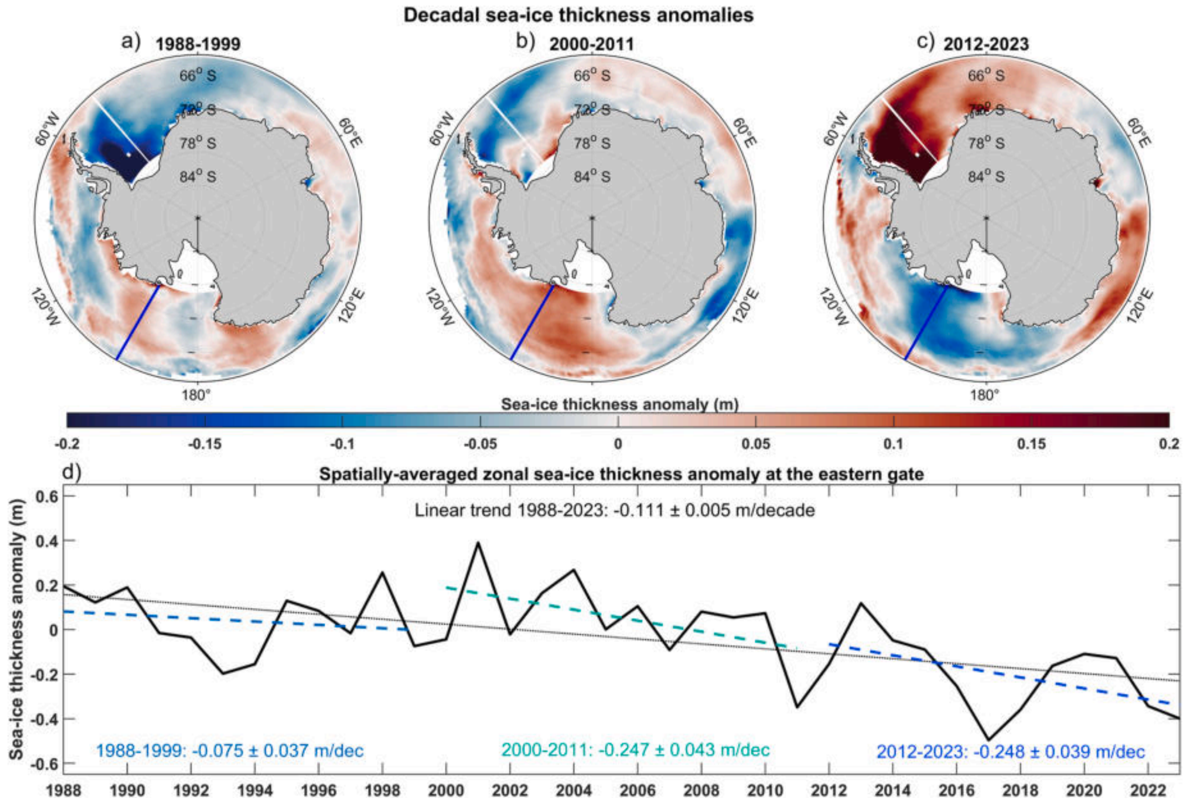

Fig. 4. Spatial distribution of the de-seasoned sea ice thickness anomalies during (a) 1988–1999, (b) 2000–2011 and (c) 2012–2023. The seasonal climatological fields of the sea ice thickness can be seen in Fig. S2b in the supplementary material; (d) Yearly values of the spatially-averaged anomalies through the selected eastern gate with trends per individual ~ decadal period (colored dashed lines) and trend for the entire time span (black dotted line). The longitudinal section of the eastern gate is indicated with a thick blue line in the spatial maps (a)–(c).

In contrast, the integrated open-ocean transport towards the Amundsen Sea showed a moderate upward trend until the late 1990s. The trend of positive transport values was interrupted in 2007 by a significant negative anomaly of approximately -77 km^3/month. Notably, 2007 was the only year in the entire record where sea ice was predominantly transported westward towards the Ross Sea (see)Table S1, resulting in an average yearly flux of around -33 km^3/month across the entire eastern gate. This anomaly was driven by the sea ice flux in the open-ocean region, which reached a peak westward transport of -155.140 km^3/month in November 2007.

3.2. Overview of prevailing sea ice dynamics in the Ross Sea

In order to gain insight into the occurring sea ice transport change throughout the different decades, we examined prevailing sea ice conditions that influence the sea ice flux across the eastern gate.

A significant decline in sea ice concentration was observed over the entire study period, at a rate of -2.831 ± 0.135 %/decade (Fig. 3d). A similar pattern was noted for sea ice thickness, which decreased by -0.111 ± 0.005 m/decade (Fig. 4d) across the eastern gate, accompanied by a slight increase in eastward sea ice drift velocity (+0.001 ± 0.0001 m/s/decade, Fig. 5d). However, these trends were not consistent across the different ~ decadal intervals.

Regarding the sea ice concentration, during 1988–1999 the eastern Ross Sea exhibited modest positive anomalies, indicating slightly higher-than-average concentrations (Fig. 3a). Early fluctuations, such as the decreases seen in 1991 and 1993, are offset by more substantial increases across the eastern gate during years like 1998 (Fig. 3d), resulting in a slight overall increase in sea ice concentration (~1 % per decade). The second period (2000-2011) marks a notable shift towards negative anomalies, revealing a decline of more than -6 (±1.164) % per decade (Fig. 3d), with an extreme anomaly in 2011 driving this downward trend. In the subsequent years, even higher negative anomalies were observed in the entire area of the eastern Ross Sea (Fig. 3c), with sea ice concentration across the eastern gate reaching its lowest recorded value of 63.531% in 2017. This resulted in an overall decline at a rate of -9.056 (±1.259) % per decade during 2012-2023.

Sea ice thickness exhibited modest positive anomalies during 1988-1999, indicating slightly thicker-than-average sea ice in the eastern Ross Sea (Fig. 4a). Moderate fluctuations with decreases in the early 90s and a rebound later in the decade resulted in a small overall decline of -0.075 (±0.037) m/decade across the eastern gate (Fig. 4d). Record high values during 2001 and 2004 led to increased positive anomalies across the majority of the eastern Ross Sea during the second period (Fig. 4b). The following years, however, marked a sharp decrease, leading up to extreme negative values in 2011 which drove much of the decadal decline (-0.247 ± 0.043 m/decade). In the most recent period (2012–2023), negative sea ice thickness anomalies persisted across the eastern Ross Sea, with substantial thinning (-0.20 m on average) observed along the eastern gate (Fig. 4c). With strong negative anomalies every consecutive year from 2014 onwards (Fig. 4d) and a record low sea ice thickness in 2017 (0.75 m), this period experienced the greatest reduction in sea ice thickness with a rate of -0.248 (±0.039) m/decade.

Regarding the zonal sea ice drift, during the first ~ decadal period the eastern Ross Sea exhibited strong positive anomalies in the coastal area, indicating higher-than-average eastward drift of coastal sea ice during 1988–1999 (Fig. 5a). Early in the decade, zonal sea ice drift velocities across the eastern gate fluctuated minimally, while a notable high positive anomaly in 1997 contributed to an overall increase of 0.003 (±0.001) m/s per decade. The second period (2000-2011) marked a shift towards negative anomalies, indicating a reduction in zonal sea

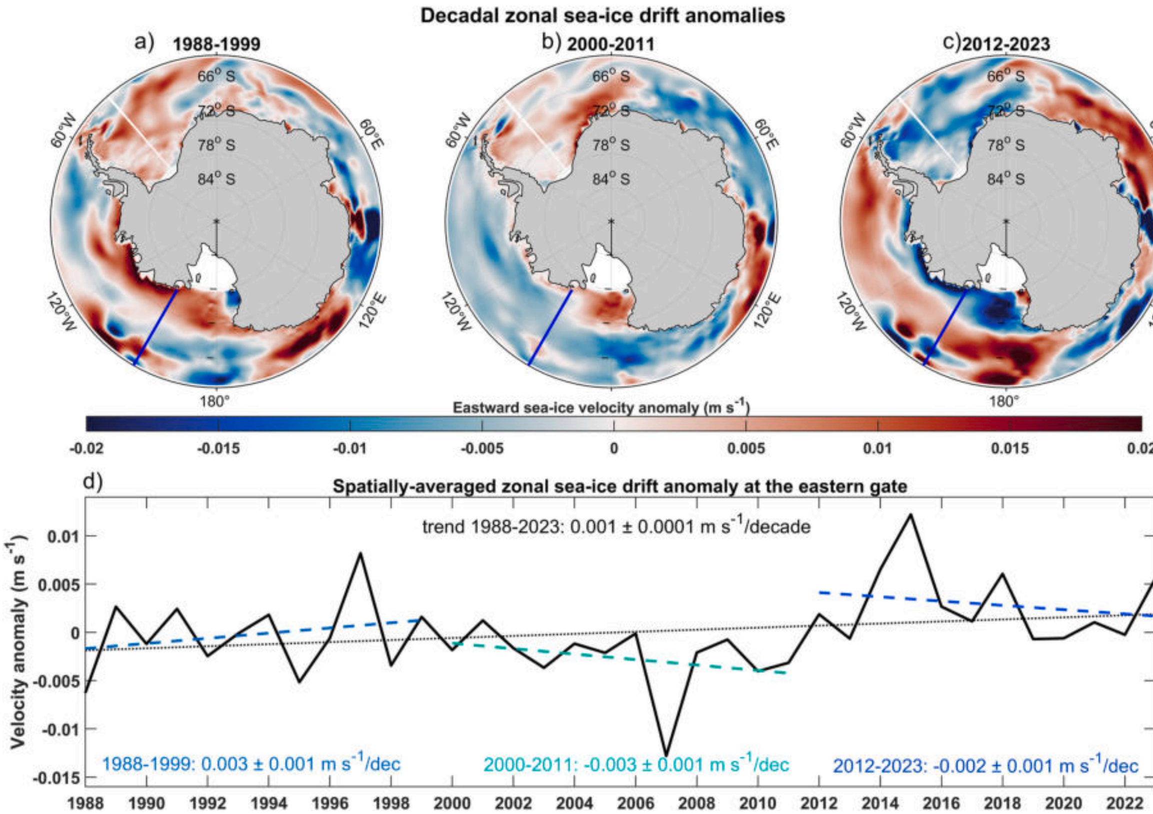

Fig. 5. Spatial distribution of the de-seasoned eastward sea ice drift anomalies during (a) 1988–1999, (b) 2000–2011 and (c) 2012–2023. The overall mean and seasonal climatological fields of the zonal sea ice drift can be seen in Fig. S2 in the supplementary material; (d) Yearly values of the spatially-averaged anomalies at the eastern gate with trends per individual ~ decadal period (colored dashed lines) and trend for the entire time span (black dotted line). The longitudinal section of the eastern gate is indicated with a thick blue line in the spatial maps (a)–(c).

ice drift velocities across the eastern Ross Sea (Fig. 5b). A record-low anomaly in 2007 (-0.013 m/s) drove much of the decline in eastward sea ice drift across the eastern gate, resulting in a negative trend of -0.003 (±0.001) m/s per decade. The most recent period (2012–2023) shows a divergence in zonal drift anomalies, with negative anomalies dominating the coastal region and positive anomalies prevailing in the open ocean (Fig. 5c). While a strong positive anomaly in 2015 briefly increased eastward sea ice drift, the overall trend was offset by subsequent negative anomalies, leading to a moderate decline in eastward drift across the eastern gate at a rate of -0.002 (±0.001) m/s per decade.

The observed shifts in sea ice concentration, thickness, and zonal drift provide first insights into the underlying conditions driving the interannual variability and abrupt changes in zonal sea ice transport (see Fig. 2 and Table S1). The pronounced decline in sea ice concentration and thickness, particularly during extreme years such as 2011 and 2017, appears to have resulted in a diminished capacity for zonal sea ice transport, especially evident in the coastal area in 2011. Furthermore, significant changes in sea ice drift, such as the strong eastward drift in 1997 and 2015, and the reversal to westward drift in 2007, seem to have contributed to intensified positive and negative transport anomalies in the open-ocean area of the eastern gate of the Ross Sea, respectively.

In order to gain further insight into the complex zonal sea ice transport, we also assessed the potential influence of large-scale teleconnections on seasonal scales. The necessity to examine seasonal shifts is evident in the climatology of the latitudinal extent of sea ice concentration (Fig. S5) along the eastern gate. During the austral summer, particularly in February, the sea ice edge at the Ross Sea eastern gate shifts significantly southward, reaching as far as 76°S in recent years. While during the austral winter (August and September), the 80% sea ice concentration level also moves southward, leading to a less compacted sea ice cover up to 68°S. A similar pattern is observed in sea ice thickness (Fig. S6), with thinning particularly evident during July, August, and September. Since 2014, sea ice thickness of just over 1.2 m has extended to 75°S, but with a notable reduction of ~25 cm at these same latitudes during the winter months compared to previous decades. Over time, both summer sea ice retreat and winter thinning have intensified, reflecting the long-term decline in sea ice extent and thickness.

3.3. Assessment of persistent large-scale forcing

To assess potential drivers on seasonal scales, we examined the influence of key large-scale teleconnection indices, namely the SOI, SAM, ASL, ZW3 and ZW3 phase, on the leading EOF mode of the zonal sea ice transport across the eastern gate during austral winter and summer.

The first EOF of the zonal sea ice transport across the eastern gate during winter accounts for ~49% of the total (detrended) variance (Fig. S9), indicating that it captures nearly half of the variability. Its temporal mode (PC 1) indicates significant interannual variability, whereas the spatial pattern reveals a meridional gradient with the northernmost (<65 deg. latitude) and the southern region of the eastern gate in opposition of phase, indicating a dipole oscillation in zonal sea ice transport during winter. This gradient manifests as a dipole oscillation, where the open-ocean (north of 65°S latitude) and the coastal region are out of phase, indicating opposing directions of sea ice transport between these areas during winter.

The correlational analysis indicates that zonal sea ice transport during winter is strongly modulated by SAM, SOI, and ASL, and to a lesser extent by ZW3 and its phase (see Fig. 6 and Table S3):

A significant negative correlation with SAM ($r = -0.57$, $p < 0.001$) suggests that negative SAM phases enhance eastward sea ice transport in the southern region of the eastern gate. During negative SAM phases, the circumpolar westerly winds are known to weaken and shift

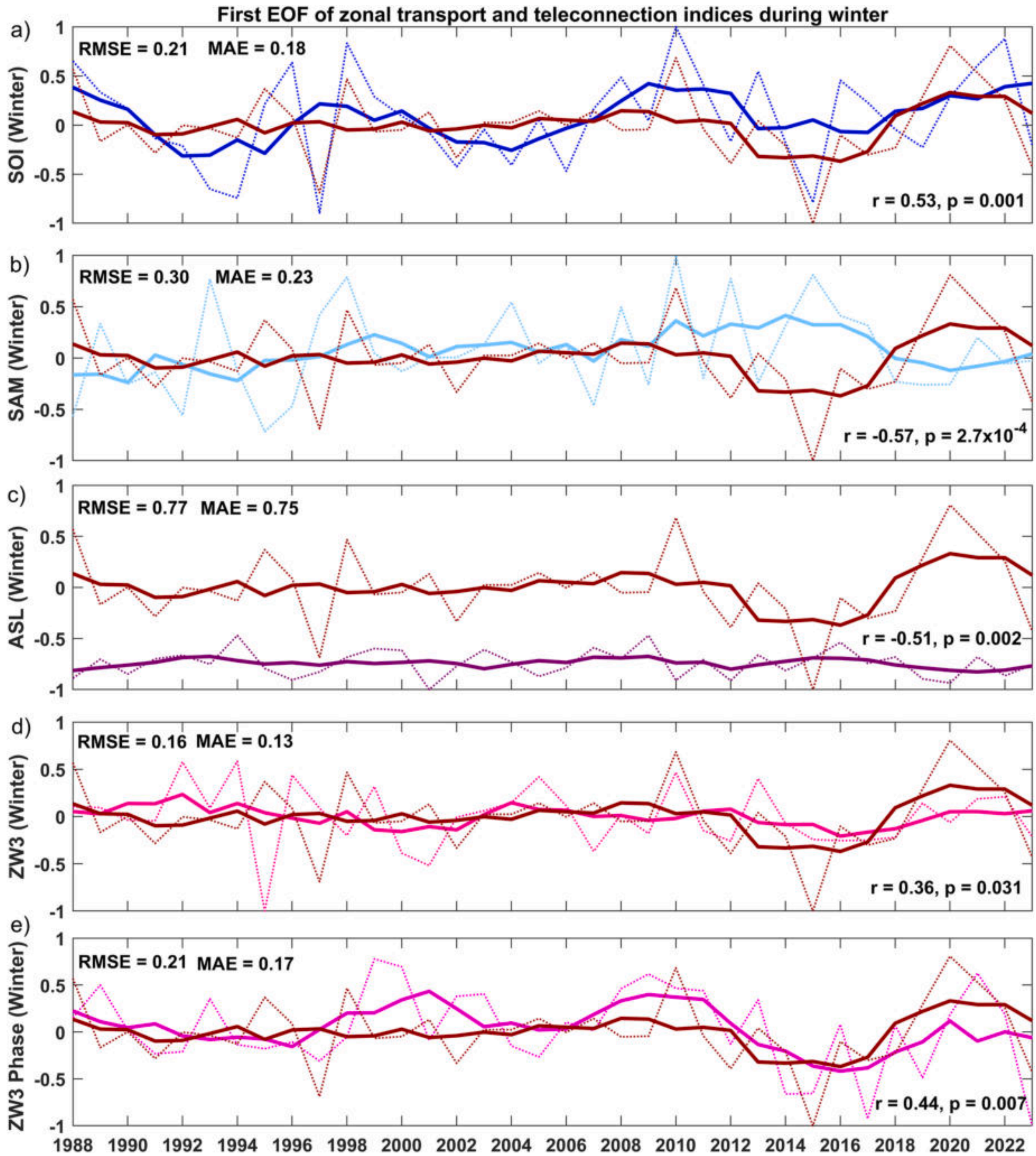

Fig. 6. Normalized time series of the first EOF mode zonal sea ice transport across the eastern gate during winter (red, dotted line) together with the (a) SOI pattern (dark blue, dotted line), (b) the SAM index (light blue, dotted line), (c) the ASL index (violet, dotted line), (d) the ZW3 magnitude (pink, dotted line) and (e) the ZW3 phase (purple, dotted line), along with their corresponding 5-year running averages (solid lines).

equatorward, reducing their dominance over the open ocean (Thompson et al., 2000). This weakening allows for greater influence of the ASL, which enhances easterly winds in the coastal region, thus further supporting eastward transport (Hosking et al., 2013). Negative SAM phases, therefore, are expected to create conditions conducive to eastward transport, especially near the coast, where ASL-driven easterlies are more prominent. Conversely, positive SAM phases are associated with stronger westerlies that shift poleward, enhancing zonal wind stress over the open ocean but potentially reducing eastward transport in coastal regions due to interference with ASL-driven easterlies (Turner et al., 2013; Raphael et al., 2016). This interaction between the poleward-shifted westerlies and the persistent easterly winds driven by the ASL creates a complex balance between eastward and westward transport across the eastern gate.

The SOI plays a similarly significant role, with a positive correlation ($r=0.53$, $p<0.05$) indicating that La Niña conditions (positive SOI) promote stronger westerly winds across the open ocean. These strengthened westerlies are expected to drive enhanced eastward sea ice transport, particularly in the open-ocean regions of the Ross Sea. La Niña conditions tend to promote atmospheric circulation patterns that favor eastward zonal sea ice transport (Holland and Kwok, 2012), reinforcing the dipole pattern observed between the northern and southern parts of the gate. This suggests that westerly winds, which are stronger during La Niña phases, effectively push sea ice eastward in the open ocean.

The ASL also exerts a significant influence, with a negative correlation ($r=-0.51$, $p<0.05$) suggesting that a deepened ASL strengthens easterly winds over the Ross Sea. These easterlies oppose the westerly-driven transport in the open ocean but drive westward sea ice

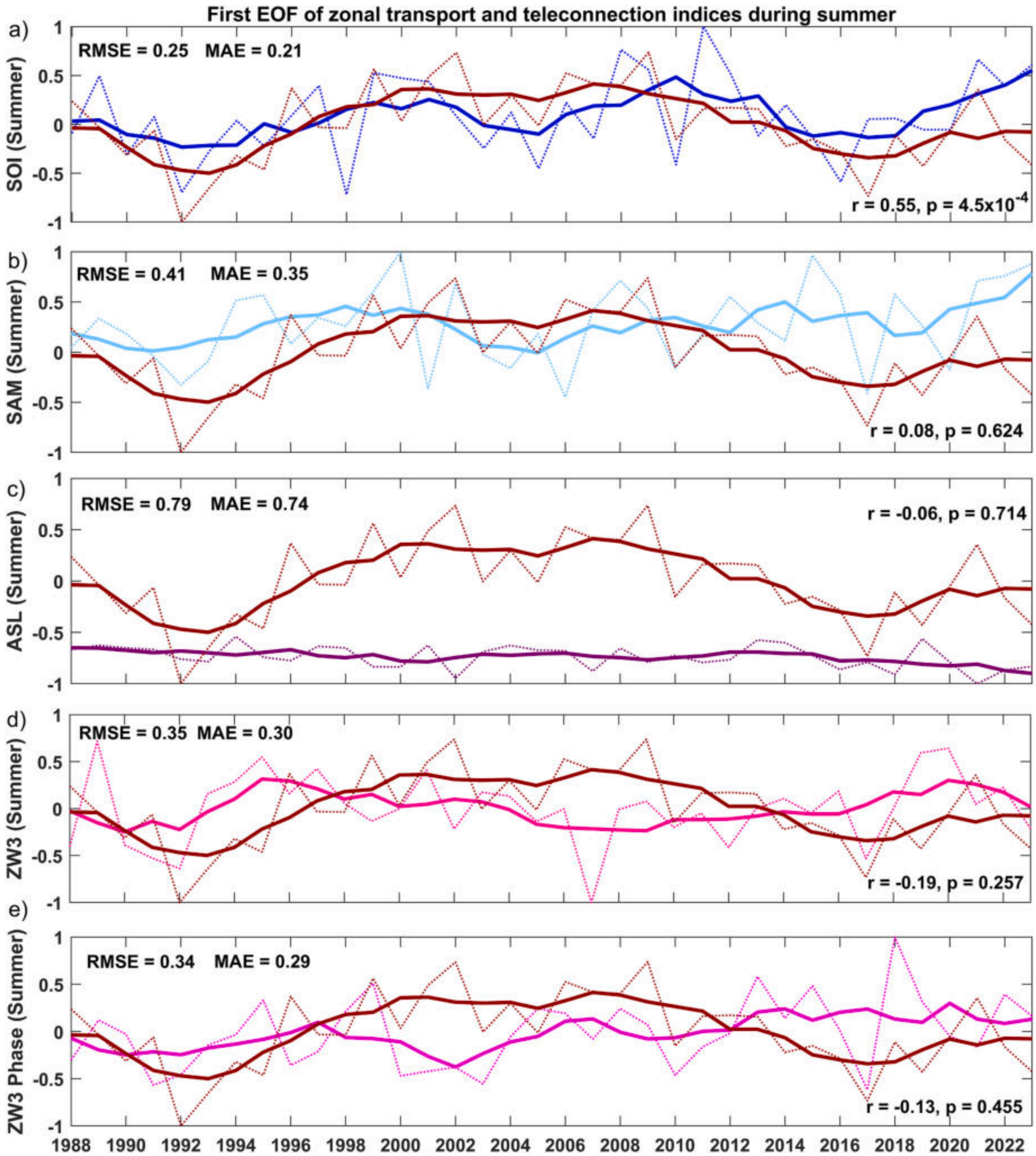

Fig. 7. Normalized time series of the first EOF mode zonal sea ice transport across the eastern gate during summer (red, dotted line) together with the (a) SOI pattern (dark blue, dotted line), (b) the SAM index (light blue, dotted line), (c) the ASL index (violet, dotted line), (d) the ZW3 magnitude (pink, dotted line) and (e) the ZW3 phase (purple, dotted line), along with their corresponding 5-year running averages (solid lines).

transport in coastal regions (Raphael et al., 2016). Thus, the ASL creates opposing wind regimes, which hinder eastward transport near the coast but have a lesser impact on the open ocean, where westerlies dominate.

In contrast, during austral summer, the first EOF of zonal sea ice transport across the eastern gate explains approximately 62% of the total variance (Fig. S10), indicating a strong dominance. The corresponding PC1 reveals three distinct periods of variability, suggesting quasi-decadal-scale fluctuations in sea ice transport. The spatial pattern is characterized by a positive in-phase increase toward the southern region of the eastern gate, indicating a more uniform response in sea ice transport during the summer months.

The dominant large-scale driver of zonal sea ice transport variability during summer is the SOI, with a statistically significant positive correlation ($r=0.55$, $p<0.001$) reflecting the influence of ENSO on atmospheric circulation patterns (Holland and Kwok, 2012). This result suggests that during La Niña phases (positive SOI), stronger westerly winds are generated across the open ocean, promoting enhanced eastward sea ice transport. These strengthened westerlies likely amplify the zonal transport of sea ice, particularly over regions with thinner and less concentrated sea ice, as atmospheric circulation associated with La Niña tends to create favorable conditions for eastward advection (Holland and Kwok, 2012).

Other teleconnections, including SAM, ASL, and ZW3, appear to play minimal roles in influencing sea ice transport during this season (see Fig. 7 and Table S3). This suggests that summer transport processes are less susceptible to the complex interplay of atmospheric forcing that characterizes winter dynamics. Thus, the positive in-phase spatial pattern observed during summer is likely driven by more uniform

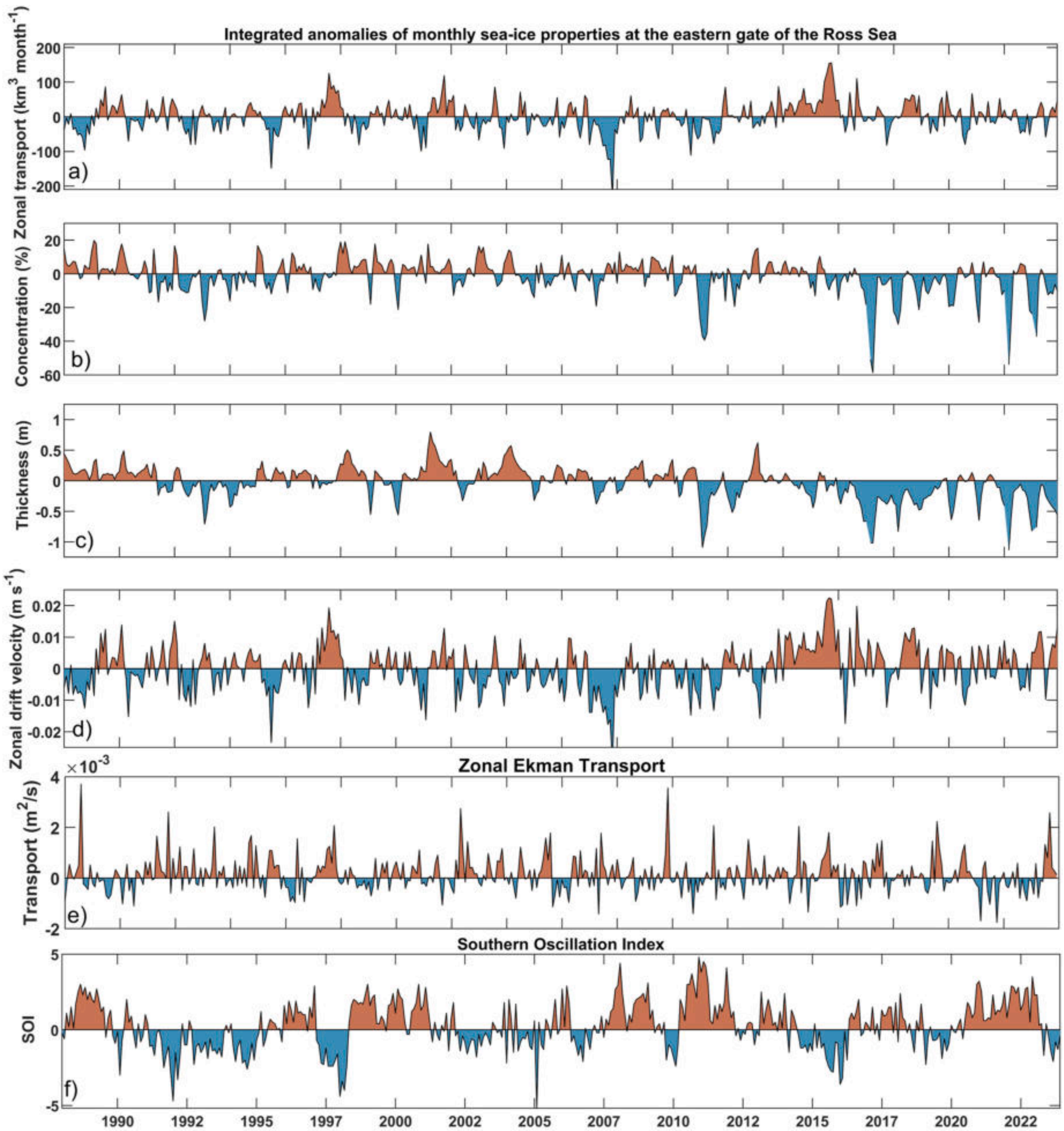

Fig. 8. Integrated monthly anomalies of the zonal sea ice transport (a) and the main conditions (b–d), as well as the zonal Ekman transport at the eastern gate of the Ross Sea alongside the monthly anomaly of the SOI (e). Positive (negative) SOI values are indicative of La Niña (El Niño) events.

processes, such as sea ice retreat and Ekman transport, which are amplified during La Niña events.

4. Discussion and conclusions

This exploratory study examines the complex dynamics of sea ice transport through the eastern gate of the Ross Sea (150°W meridian) from 1988 to 2023, revealing substantial temporal and spatial variations. Although we observe a weak overall trend of increased eastward sea ice transport across the gate, this general rise conceals significant regional and temporal variations, which have important implications for understanding sea ice dynamics in the Ross Sea.

The analysis of zonal sea ice transport trends over the past four decades revealed diverging patterns between the coastal and open-ocean regions. While there was an overall modest increase in eastward transport across the entire eastern gate (~3.7 km^3/month per decade), coastal regions experienced a significant rise in sea ice import during the early 2000s, followed by a steep decline post-2011. Conversely, open-ocean transport showed a moderate increase towards the Amundsen Sea until the late 1990s, interrupted by a notable reversal in 2007. This shift aligns with increased wind stress variability and changes in sea ice conditions (Figs. 3–5), as corroborated by prior findings that highlight wind-driven trends in Antarctic sea ice motion (Holland and Kwok, 2012).

Abrupt changes and record anomalies in zonal sea ice transport were largely explained by underlying sea ice conditions, as trends in concentration, thickness, and zonal drift varied across the three ~decadal periods. The early years (1988-1999) displayed relatively stable or modest positive anomalies. However, from 2000 to 2011, there was a marked shift towards negative sea ice concentration and thickness anomalies, with extreme declines in 2011 and 2017. In the most recent period (2012-2023), these negative trends intensified, while shifts in sea ice drift contributed to intensified transport anomalies, particularly in the open ocean. Notable examples included strong eastward drift in

1997 and 2015, and an extreme westward sea ice drift in 2007.

The influence of zonal wind stress (see Fig. S11 and S12) and Ekman transport (Fig. 8d, S11 and S13) emerges as a significant factor in explaining these patterns, particularly in recent years. The thinning of sea ice in the open ocean appears to have rendered the region more susceptible to atmospheric forcing. Relevant studies in the Arctic have shown that thinner and less compact sea ice is more easily influenced by wind-driven processes (Kwok, 2011; Petty et al., 2018), further enhancing eastward advection. Thinner sea ice, especially during summer months, offers less resistance to atmospheric forcing, which allows for stronger wind-driven transport. This is particularly evident in regions where sea ice concentration and thickness have declined, amplifying the role of zonal wind stress and Ekman transport (see Fig. 8 and supplementary Figs. S11-S13). Kwok (2011) specifically noted that as sea ice becomes thinner, its sensitivity to changes in wind and ocean currents increases, leading to higher variability in sea ice drift and transport patterns. These findings suggest that ongoing changes in sea ice thickness and concentration will likely amplify the role of wind-driven processes in shaping future sea ice dynamics in the Ross Sea.

The complex sea ice transport dynamics were found to be influenced by large-scale atmospheric drivers on seasonal scales. Winter transport variability seems to be driven by teleconnections, particularly SAM, SOI, ASL, and ZW3, with SOI dominating during summer and correlating with enhanced eastward transport during La Niña phases. Notably, some of the strongest El Niño events on record took place in 1997-1998, 2005 and 2014-2016 (Fig. 8f) which correlates with the zonal Ekman transport across the eastern gate (Fig. 8e). The ASL, probably modulated by SOI, reinforces this effect through stronger easterlies. Although ZW3 has a more subtle influence, it adds complexity to the overall wind stress patterns.

It is important to note that different teleconnections can interact through interconnected underlying mechanisms (Fogt et al., 2011). Future work should focus on how synchronous in-phase teleconnections might drive sea ice dynamics and how one teleconnection, such as the SOI, can precondition the strength of others like the SAM or the ASL. Understanding the role of these large-scale teleconnections is essential for predicting future changes in sea ice distribution and evaluating their broader impacts on global climate systems and marine ecosystems.

The observed changes in sea ice dynamics are intricately linked with regional oceanographic conditions, notably influencing the salinity levels in the Ross Sea. Silvano et al. (2020) highlighted how decreased sea ice import from the Amundsen Sea during 2015-2018 has contributed to increased local sea ice formation and subsequent changes in the salinity field of the Ross Sea, affecting the characteristics of High Salinity Shelf Water (HSSW) and, in turn, the Antarctic Bottom Water (AABW). These changes are crucial as they impact the global thermohaline circulation and the storage of heat and carbon in the abyssal ocean.

Looking forward, future research should focus on enhancing our understanding of these dynamic processes, particularly in relation to ocean-driven changes such as ocean heat content and variations in large-scale circulatory systems like the Ross Gyre. Interactions between sea ice and adjacent features, such as the Ross Ice Shelf, should also be explored in greater detail to better understand the implications of sea ice variability for the region's broader oceanographic and climatic conditions.

In conclusion, this work provides foundational insights into the dynamic nature of sea ice transport across the eastern gate of the Ross Sea, highlighting the importance of large-scale teleconnections, zonal wind stress, and Ekman transport in driving these processes. The observed sensitivity of sea ice to atmospheric forcing, particularly in regions with thinner and less compact ice, underscores the need for continued monitoring and further research into the evolving relationship between sea ice, wind stress, and oceanic processes. As climate change continues to impact the Southern Ocean, understanding these complex interactions will be crucial for predicting future sea ice behavior and its broader implications for the global climate system.

CRediT authorship contribution statement

Naomi Krauzig: Writing – review & editing, Writing – original draft, Visualization, Validation, Methodology, Investigation, Formal analysis, Data curation, Conceptualization. **Daniela Flocco:** Writing – review & editing, Supervision, Methodology, Data curation, Conceptualization. **Stefan Kern:** Writing – review & editing. **Enrico Zambianchi:** Writing – review & editing, Supervision, Project administration, Funding acquisition.

Financial support

NK, DF and EZ received support from the Italian National Program for Antarctic Research through the project “Effect of the eaSTern inflow of water on the ROss Sea salinity field variability (ESTRO)", PNRA18_00258.

Declaration of competing interest

The authors declare that they have no known competing financial interests or personal relationships that could have appeared to influence the work reported in this paper.

Acknowledgements

The authors acknowledge the usage of two freely-available MATLAB toolboxes: a) M_Map: A mapping package for MATLAB (version 1.4m), developed by Pawlowicz (2020), which is available online at www.eoas.ubc.ca/~rich/map.html.

b) CDT: the Climate Data Toolbox for MATLAB (version 1.01), developed by Greene et al. (2019), which can be accessed at https://github.com/chadagreene/CDT.

Appendix A. Supplementary data

Supplementary data to this article can be found online at https://doi.org/10.1016/j.dsr2.2024.105428.

Data availability

Satellite-derived sea ice concentration data are available from the National Snow and Ice Data Center (NSIDC) Distributed Active Archive Center (https://doi.org/10.5067/INAWUWO7QH7B). Sea ice motion, concentration and thickness data from the Global Ice-Ocean Modeling and Assimilation System (GIOMAS) are obtainable by the Polar Science Center of the University of Washington (https://psc.apl.washington.edu). The SAM, ASL and SOI teleconnection indices are available from BAS (http://www.nerc-bas.ac.uk/icd/gjma/sam.html and https://scotthosking.com/asl_index) and from the National Center for Atmospheric Research (NCAR; https://climatedataguide.ucar.edu/climate-data), respectively. All data analyses and representations were conducted using MATLAB 2023b (available at https://it.mathworks.com/products/matlab.html). The generated scripts are available upon reasonable request from the first author.

References

Abernathey, R., Cerovecki, I., Holland, P., et al., 2016. Water-mass transformation by sea ice in the upper branch of the Southern Ocean overturning. Nat. Geosci. 9, 596–601. https://doi.org/10.1038/ngeo2749.

Assmann, K.M., Hellmer, H.H., Jacobs, S.S., 2005. Amundsen Sea ice production and transport. J. Geophys. Res. 110, C12013. https://doi.org/10.1029/2004JC002797.

Bjoernsson, H., Venegas, S., 1997. A Manual for EOF and SVD Analyses of Climate Data, vol. 97. McGill University, pp. 1–52. CCGCR Report.

Coggins, J.H.J., McDonald, A.J., 2015. The influence of the Amundsen sea low on the winds in the Ross sea and surroundings: insights from a synoptic climatology. J. Geophys. Res. 120, 2167–2189.

Eayrs, C., Li, X., Raphael, M.N., Holland, D.M., 2021. Rapid decline in Antarctic sea ice in recent years hints at future change. Nat. Geosci. 14 (7), 460–464. https://doi.org/10.1038/s41561-021-00768-3.
Eayrs, C., Holland, D., Francis, D., Wagner, T., Kumar, R., Li, X., 2019. Understanding the seasonal cycle of Antarctic sea ice extent in the context of longer-term variability. Rev. Geophys. 57, 1037–1064. https://doi.org/10.1029/2018RG000631.
Fogt, R.L., Bromwich, D.H., Hines, K.M., 2011. Understanding the SAM influence on the south pacific ENSO teleconnection. Clim. Dynam. 36, 1555–1576. https://doi.org/10.1007/s00382-010-0905-0.
Fogt, R.L., Dalaiden, Q., Zarembka, M.S., 2022. Understanding differences in Antarctic sea-ice-extent reconstructions in the Ross, amundsen, and bellingshausen seas since 1900. Past Glob. Chang. Magaz. 30 (22), 74–75. https://doi.org/10.22498/pages.30.2.74.
Goyal, R., Jucker, M., Sen Gupta, A., Hendon, H., England, M.H., 2021. Zonal wave 3 pattern in the Southern Hemisphere generated by tropical convection. Nat. Geosci. 14, 732–738. https://doi.org/10.1038/s41561-021-00811-3.
Goyal, R., Jucker, M., Sen Gupta, A., England, M.H., 2022. A new zonal wave-3 index for the southern Hemisphere. J. Clim. 35 (15), 5137–5149. https://doi.org/10.1175/JCLI-D-21-0927.1.
Greene, C.A., Thirumalai, K., Kearney, K.A., Delgado, J.M., Schwanghart, W., Wolfenbarger, N.S., et al., 2019. The climate data toolbox for MATLAB. G-cubed 20, 3774–3781. https://doi.org/10.1029/2019GC008392.
Guo, G., Gao, L., Shi, J., 2020. Modulation of dense shelf water salinity variability in the western Ross Sea associated with the Amundsen Sea Low. Environ. Res. Lett. 16, 014004.
Haumann, F.A., Gruber, N., Münnich, M., Frenger, I., Kern, S., 2016. Sea-ice transport driving. Sea ice transport driving Southern Ocean salinity and its recent trends. Nature 537 (7618), 89–92. https://doi.org/10.1038/nature19101.
Hersbach, H., Bell, B., Berrisford, P., Biavati, G., Horányi, A., Muñoz Sabater, J., Nicolas, J., Peubey, C., Radu, R., Rozum, I., Schepers, D., Simmons, A., Soci, C., Dee, D., Thépaut, J.-N., 2023a. ERA5 monthly averaged data on pressure levels from 1940 to present. Copernicus Clim. Chang. Serv. (C3S) Clim. Data Store (CDS). https://doi.org/10.24381/cds.6860a573.
Hersbach, H., Bell, B., Berrisford, P., Biavati, G., Horányi, A., Muñoz Sabater, J., Nicolas, J., Peubey, C., Radu, R., Rozum, I., Schepers, D., Simmons, A., Soci, C., Dee, D., Thépaut, J.-N., 2023b. ERA5 monthly averaged data on single levels from 1940 to present. Copernicus Clim. Chang. Serv. (C3S) Clim. Data Store (CDS). https://doi.org/10.24381/cds.f17050d7.
Holland, P.R., Bruneau, N., Enright, C., Kurtz, N.T., Losch, M., Kwok, R., 2014. Modeled trends in Antarctic sea ice thickness. J. Clim. 27, 3784–3801. https://doi.org/10.1175/JCLI-D-13-00301.1.
Holland, P., Kwok, R., 2012. Wind-driven trends in Antarctic sea-ice drift. Nat. Geosci. 5, 872–875. https://doi.org/10.1038/ngeo1627.
Hosking, J.S., Orr, A., Marshall, G.J., Turner, J., Phillips, T., 2013. The influence of the Amundsen–Bellingshausen Seas Low on the climate of West Antarctica and its representation in coupled climate model simulations. J. Clim. 26 (17), 6633–6648. https://doi.org/10.1175/JCLI-D-12-00813.1.
IPCC SROCC, 2020. IPCC Special Report on the Ocean and Cryosphere in a Changing Climate. Cambridge University Press. https://doi.org/10.1017/9781009157964.
Jena, B., Kshitija, S., Bajish, C.C., Turner, J., Holmes, C., Wilkinson, J., et al., 2024. Evolution of Antarctic sea ice ahead of the record low annual maximum extent in September 2023. Geophys. Res. Lett. 51, e2023GL107561. https://doi.org/10.1029/2023GL107561.
Kendall, M., 1962. Rank Correlation Methods. Hafner Publishing Company, New York.
Kern, S., 2009. Wintertime Antarctic coastal polynya area: 1992–2008. Geophys. Res. Lett. 36, L14501.
Kern, S., Khvorostovsky, K., Skourup, H., Rinne, E., Parsakhoo, Z.S., Djepa, V., Wadhams, P., Sandven, S., 2015. The impact of snow depth, snow density and ice density on sea ice thickness retrieval from satellite radar altimetry: results from the ESA-CCI Sea Ice ECV Project Round Robin Exercise. Cryosphere 9, 37–52. https://doi.org/10.5194/tc-9-37-2015.
Kwok, R., 2011. Observational assessment of Arctic Ocean sea ice motion, export, and thickness in CMIP3 climate simulations. J. Geophys. Res.: Oceans 116, C00D05. https://doi.org/10.1029/2011JC007004.
Liao, S., Luo, H., Wang, J., Shi, Q., Zhang, J., Yang, Q., 2022. An evaluation of Antarctic sea-ice thickness from the Global Ice-Ocean Modeling and Assimilation System based on in situ and satellite observations. Cryosphere 16, 1807–1819. https://doi.org/10.5194/tc-16-1807-2022.
Lindsay, R.W., Zhang, J., 2006. Assimilation of ice concentration in an ice–ocean model. J. Atmos. Ocean. Technol. 23, 742–749. https://doi.org/10.1175/jtech1871.1.
Lüpkes, C., Birnbaum, G., 2005. Surface drag in the arctic marginal Sea-ice zone: a comparison of different parameterisation concepts. Boundary-Layer Meteorol. 117, 179–211. https://doi.org/10.1007/s10546-005-1445-8.
Mann, H., 1945. Nonparametric tests against trend. Econometrica 13 (3), 245–259.
Marshall, G.J., 2003. Trends in the southern annular mode from observations and reanalyses. J. Clim. 16, 4134–4143.
Martin, S., Drucker, R.S., Kwok, R., 2007. The areas and ice production of the western and central Ross Sea polynyas, 1992–2002, and their relation to the B-15 and C-19 iceberg events of 2000 and 2002. J. Mar. Syst. 68, 201–214. https://doi.org/10.1016/j.jmarsys.2006.11.008.
Massom, R.A., Scambos, T.A., Bennetts, L.G., Reid, P., Squire, V.A., Stammerjohn, S.E., 2018. Antarctic ice shelf disintegration triggered by sea ice loss and ocean swell. Nature 558, 383–389.
Massom, R.A., Stammerjohn, S.E., 2010. Antarctic sea ice change and variability—physical and ecological implications. Pol. Sci. 4, 149–186. https://doi.org/10.1016/j.polar.2010.05.001.
Massonnet, F., Mathiot, P., Fichefet, T., Goosse, H., Beatty, C.K., Vancoppenolle, M., Lavergne, T., 2013. A model reconstruction of the Antarctic sea ice thickness and volume changes over 1980–2008 using data assimilation. Ocean Model. 64, 67–75. https://doi.org/10.1175/JCLI-D-13-00301.1.
Meehl, G.A., Arblaster, J.M., Chung, C.T.Y., Holland, M.M., DuVivier, A., 2019. Sustained ocean changes contributed to sudden Antarctic sea ice retreat in late 2016. Nat. Commun. 10 (1), 14. https://doi.org/10.1038/s41467-018-07865-9, 2019.
Nihashi, S., Ohshima, K.I., 2015. Circumpolar mapping of antarctic coastal polynyas and landfast sea ice: relationship and variability. J. Clim. 28, 3650–3670. https://doi.org/10.1175/JCLI-D-14-00369.1.
Nihashi, S., Ohshima, K.I., Tamura, T., 2017. Sea-ice production in Antarctic coastal polynyas estimated from AMSR2 data and its validation using AMSR-E and SSM/I-SSMIS data. IEEE J. Sel. Top. Appl. Earth Obs. Rem. Sens. 10 (9), 3912–3922. https://doi.org/10.1109/JSTARS.2017.2731995.
Nihashi, S., Ohshima, K.I., Tamura, T., 2024. Reconstruct the AMSR-E/2 thin ice thickness algorithm to create a long-term time series of sea-ice production in Antarctic coastal polynyas. Polar Sci. 39, 100978. https://doi.org/10.1016/j.polar.2023.100978.
Ohshima, K., Fukamachi, Y., Williams, G., et al., 2013. Antarctic Bottom Water production by intense sea-ice formation in the Cape Darnley polynya. Nat. Geosci. 6, 235–240. https://doi.org/10.1038/ngeo1738.
Parkinson, C.L., Cavalieri, D.J., 2012. Antarctic sea ice variability and trends, 1979–2010. Cryosphere 6, 871–880. https://doi.org/10.5194/tc-6-871-2012.
Parkinson, C.L., DiGirolamo, N.E., 2021. Sea ice extents continue to set new records: arctic, Antarctic, and global results. Remote Sens. Environ. 267, 112753. https://doi.org/10.1016/j.rse.2021.112753, 2021.
Pawlowicz, R., 2020. M_Map: a mapping package for MATLAB. Comput. Software. www.eoas.ubc.ca/~rich/map.html.
Petty, A.A., Schröder, D., Feltham, D.L., 2018. Sea ice circulation around the Beaufort Gyre: the changing role of wind forcing and the sea ice state. J. Geophys. Res.: Oceans 123 (11), 8044–8065. https://doi.org/10.1002/2015JC010903.
Purich, A., Doddridge, E.W., 2023. Record low Antarctic sea ice coverage indicates a new sea ice state. Commun. Earth Environ. 4 (1), 1–9. https://doi.org/10.1038/s43247-023-00961-9.
Raphael, M.N., 2004. A zonal wave 3 index for the Southern Hemisphere. Geophys. Res. Lett. 31, L23212. https://doi.org/10.1029/2004GL020365.
Raphael, M.N., Marshall, G.J., Turner, J., Fogt, R.L., Schneider, D., Dixon, D.A., Hosking, J.S., Jones, J.M., Hobbs, W.R., 2016. The Amundsen Sea Low: variability, change, and impact on antarctic climate. Bull. Am. Meteorol. Soc. 97, 111–121.
Raphael, M.N., Marshall, G.J., Turner, J., Fogt, R.L., Schneider, D., Dixon, D.A., et al., 2016. The Amundsen Sea Low: variability, change, and impact on antarctic climate. Bull. Am. Meteorol. Soc. 97 (1), 111–121. https://doi.org/10.1175/BAMS-D-14-00018.1.
Rintoul, S.R., 2007. Rapid freshening of antarctic Bottom water formed in the Indian and pacific oceans. Geophys. Res. Lett. 34, L06606.
Rysgaard, S., Bendtsen, J., Delille, B., Dieckmann, G.S., Glud, R.N., Kennedy, H., Mortensen, J., Padimitriou, S., Thomas, D.N., Tison, J.-L., 2011. Sea ice contribution to the air-sea CO2 exchange in the Arctic and Southern Oceans. Tellus B 63, 823–830.
Schlosser, E., Haumann, F.A., Raphael, M.N., 2018. Atmospheric influences on the anomalous 2016 Antarctic sea ice decay. Cryosphere 12, 1103–1119. https://doi.org/10.5194/tc-12-1103-2018.
Schroeter, S., O'Kane, T.J., Sandery, P.A., 2023. Antarctic sea ice regime shift associated with decreasing zonal symmetry in the Southern Annular Mode. Cryosphere 17, 701–717. https://doi.org/10.5194/tc-17-701-2023.
Shi, Q., Yang, Q., Mu, L., Wang, J., Massonnet, F., Mazloff, M.R., 2021. Evaluation of sea-ice thickness from four reanalyses in the Antarctic Weddell Sea. Cryosphere 15, 31–47. https://doi.org/10.5194/tc-15-31-2021.
Silvano, A., Foppert, A., Rintoul, S.R., et al., 2020. Recent recovery of Antarctic Bottom water formation in the Ross Sea driven by climate anomalies. Nat. Geosci. 13, 780–786. https://doi.org/10.1038/s41561-020-00655-3.
Smith Jr., W.O., Sedwick, P.N., Arrigo, K.R., Ainley, D.G., Orsi, A.H., 2012. The Ross Sea in a sea of change. Oceanography 25 (3), 90–103. https://doi.org/10.5670/oceanog.2012.80.
Stroeve, J.C., Jenouvrier, S., Campbell, G.G., Barbraud, C., Delord, K., 2016. Mapping and assessing variability in the Antarctic marginal ice zone, pack ice and coastal polynyas in two sea ice algorithms with implications on breeding success of snow petrels. Cryosphere 10, 1823–1843. https://doi.org/10.5194/tc-10-1823-2016.
Stuecker, M.F., Bitz, C.M., Armour, K.C., 2017. Conditions leading to the unprecedented low Antarctic sea ice extent during the 2016 austral spring season. Geophys. Res. Lett. 44, 9008–9019.
Tamura, T., Ohshima, K.I., Fraser, A.D., Williams, G.D., 2016. Sea ice production variability in Antarctic coastal polynyas. J. Geophys. Res. Oceans 121, 2967–2979.
Turner, J., Holmes, C., Caton Harrison, T., Phillips, T., Jena, B., Reeves-Francois, T., et al., 2022. Record low Antarctic sea ice cover in February 2022. Geophys. Res. Lett. 49, e2022GL098904.
Turner, J., Hosking, J.S., Bracegirdle, T.J., Marshall, G.J., Phillips, Tony, 2015. Recent changes in Antarctic sea ice. Phil. Trans. R. Soc. A 37320140163. https://doi.org/10.1098/rsta.2014.0163.
Thompson, D.W., Wallace, J.M., Hegerl, G.C., 2000. Annular modes in the extratropical circulation. Part II. Trends. J. Clim. 13, 1018–1036.
Turner, J., Phillips, T., Hosking, J.S., Marshall, G.J., Orr, A., 2013. The Amundsen Sea Low. Int. J. Climatol. 33 (7), 1818–1829. https://doi.org/10.1002/joc.3558.
Van Achter, G., Fichefet, T., Goosse, H., Moreno-Chamarro, E., 2022. Influence of fast ice on future ice shelf melting in the Totten Glacier area, East Antarctica. Cryosphere 16, 4745–4761. https://doi.org/10.5194/tc-16-4745-2022.

Wang, G., Hendon, H.H., Arblaster, J.M., Lim, E.-P., Abhik, S., van Rensch, P., 2019. Compounding tropical and stratospheric forcing of the record low Antarctic sea-ice in 2016. Nat. Commun. 10, 13. https://doi.org/10.1038/s41467-018-07689-7.
Wang, J., Luo, H., Yu, L., Li, X., Holland, P.R., Yang, Q., 2023. The impacts of combined SAM and ENSO on seasonal Antarctic sea ice changes. J. Clim. 36, 3553–3569. https://doi.org/10.1175/JCLI-D-22-0679.1.
Zhang, J., Rothrock, D.A., 2003. Modeling global sea ice with a thickness and enthalpy distribution model in generalized curvilinear coordinates. Mon. Weather Rev. 131 (5), 681–697. https://doi.org/10.1175/1520-0493(2003)131%3C0845:MGSIWA%3E2.0.CO;2.